Local structure study on magnetostrictive material $Tb_{1-x}Dy_xFe_2$

Tieyan Chang,[1,2] Chao Zhou,[1] Kaige Chang,[1] Bin Wang,[3] Qian Shi,[1] Kaiyun Chen,[1] Yu-Sheng Chen,[2] Yang Ren[4] and Sen Yang[1]*

[1] *School of Science, MOE Key Laboratory for Nonequilibrium Synthesis and Modulation of Condensed Matter, Xi'an Jiaotong University, Xi'an 710049, China.*

[2] *NSF's ChemMatCARS, The University of Chicago, Lemont, IL, 60439, USA*

[3] *Shaanxi Key Laboratory of Energy Chemical Process Intensification, School of Chemical Engineering and Technology, Xi'an Jiaotong University, Xi'an, 710049, China*

[4] *X-ray Science Division, Advanced Photon Source, Argonne National Laboratory, Lemont, IL, 60439, USA*

* Email: yang.sen@xjtu.edu.cn

ABSTRACT

$Tb_{1-x}Dy_xFe_2$ system has attracted lots of research interests due to the large magnetostrictive effect. The crystal structures and physical properties have been well studied, but researches on their local structures are still rare. In this work, the local structure of $Tb_{1-x}Dy_xFe_2$ samples was studied using the pair distribution function and x-ray absorption spectroscopy techniques. The results demonstrate that the system owns the same local crystal symmetry with its average structure in the ferromagnetic phase, and the crystal lattice of system is more ordered with increasing Dy content, indicating that the Dy-rich tetragonal phase is more stable than the Tb-rich rhombohedral phase. The different roles of metallic bonds in affecting the crystal lattice are presented. The weak Fe_1-Fe_2 bonds influenced by local environment such as local stress from randomly distributed nanodomains could originate the anomalies in the lattice, resulting in the more ordered and stable Dy-rich phase than the Tb-rich phase.

Keywords: magnetostriction, local structure, structure transition, morphotropic phase boundary

I. INTRODUCTION

Magnetostrictive materials have been widely studied for their essential use as actuators and sensors, and researches were carried out on the mechanism of magnetostriction.[1-3] Lots of studies show that the ferromagnetic phase transition is coupled with crystal structural change yielding the symmetry lowering which conforms to the spontaneous magnetization.[4-7] The magnetostrictive effect is ascribed to the crystallographic domain-switching which is also the switching of magnetic domains driven by applied magnetic field.[8,9] Based on this first-order magnetoelastic phase transition, the magnetic morphotropic phase boundary (MPB) was proposed and studied in Laves compounds RT_2 (R = rare-earth, T = Co, Fe) to achieve highly improved magnetostrictive response.[10,11] The improved magnetostrictive effect in RT_2 alloys is believed to arise from the coexistence of two different crystal structures near MPB. For example, the rhombohedral distortion in Tb-rich side in $Tb_{1-x}Dy_xFe_2$ is remarkably reduced by increasing Dy content and the tetragonal distortion is then induced, and enhanced magnetostrictive effect is observed in the intermediate compositions near the rhombohedral-tetragonal phase boundary, i.e. the MPB.[8] Similar anomalous behaviors and mechanism of magnetostriction were also reported in other RT_2 systems.[11-13]

These studies evidence that the crystal structures play important roles in determining the magnetostriction. Some recent works report the developments in the mechanism of magnetostriction: the breaking of cubic symmetry in nanoscale is reported and believed to generate large magnetostrictive response;[14,15] and theoretical studies show the essential influence of local composition distribution on magnetostrictive effect in Fe-Ga systems.[16,17] These works indicate that the properties are not only attributed to macroscopic crystal structure, but also great affected by the local structure. However, detailed studies on the local structure of $Tb_{1-x}Dy_xFe_2$ system are still rare.

For decades, detecting the local structure becomes more feasible and easier with the developments of synchrotron-based pair distribution functions (PDF) and X-ray absorption spectroscopy (XAS) techniques. The PDF is regarded as a powerful tool to study the local

structure in amorphous and liquids, then it was extended to crystallized systems[18,19] which evokes that PDF could also be appropriate for studying the local structure in other crystallized systems like RT_2. Besides, the XAS is another method widely used in probing the local structure,[20] which was also applied on Fe-Ga materials to study the origin of magnetostriction.[21,22] Additionally, the XAS was well developed to probe the chemical environments and electronic structure of the absorption atoms, which can help to understand the rare-earths replacement in RT_2.

In this letter we address the investigations on the local structure of crystallized $Tb_{1-x}Dy_xFe_2$ alloys using the PDF and XAS techniques. The local structural evolutions by changing temperature of $Tb_{0.4}Dy_{0.6}Fe_2$ composition reported in Ref. 8 are studied and discussed. Moreover, the effects of Dy substitution on the electronic structure of system are studied. The Fe_1-Fe_2 bond in rhombohedral structure is believed to play an essential role in determining the lattice characters of the system.

II. EXPERIMENTAL SECTION

Polycrystalline $Tb_{1-x}Dy_xFe_2$ (x = 0, 0.6, and 1) alloys were prepared using arc-melting with high-purity Tb, Dy and Fe in argon atmosphere for six times to ensure the homogeneity. Ingots were finely grounded for synchrotron x-ray measurements at the Advanced Photon Source, Argonne National Laboratory. Powder x-ray diffraction (XRD) was performed at beamline 15-ID-D with λ=0.41328 Å. X-ray total scatterings of PDF were collected at beamline 11-ID-C with λ=0.11725 Å. XAS samples were mixed with boron nitride powder and pelletized to optimized thickness. XAS were employed at beamline 20-BM-B in the transmission mode on samples at Fe *K*-edge, with energy calibration for each spectrum made by performing simultaneous measurements on a reference metal foil. Rietveld and PDF refinements were performed using GSAS[23,24] and PDFgui[25], respectively. XAS data was analyzed using Athena and Artemis.[26]

III. RESULTS AND DISCUSSIONS

In Figure 1(a) we show the room temperature XRD for the $Tb_{0.4}Dy_{0.6}Fe_2$ composition to obtain its average crystal structure. The diffraction pattern is refined using a rhombohedral space group $R\bar{3}m$ as reported,[11,14] and the results confirm the structure model. The rhombohedral distortion comes from the slightly elongation along the [111] direction of the $MgCu_2$-type cubic cell, which is consistent with the easy axis of magnetization $\boldsymbol{M_S}$.[27] The XRD results for binary compositions $TbFe_2$ and $DyFe_2$ are shown in Figure S1, in which the samples exhibit rhombohedral and tetragonal structure, respectively. The magnetostrictive response would be greatly enhanced near the boundary separating the rhombohedral ($\boldsymbol{M_S}$ || [111]) and tetragonal ($\boldsymbol{M_S}$ || [001]) structures in RT_2 systems like $Tb_{1-x}Dy_xFe_2$ and $Tb_{1-x}Dy_xCo_2$.[8,11]

Room temperature PDF measurements were performed on samples and the results are shown in Fig. 1(b). The spectrum (range of 2~6 Å) for $Tb_{0.4}Dy_{0.6}Fe_2$ is fitted and space group $R\bar{3}m$ is obtained (shown in Figure S2), which reveals that the sample owns the same symmetry for both local and average structure at room temperature. The PDF spectra for all samples show four main peaks within the displayed range: peak at 2.6 Å is due to the nearest neighbor Fe-Fe coordination; peaks at 4.78 Å and 5.23 Å represent for the second and third Fe-Fe shells; and the peak at 3.07 Å corresponds to the R-Fe metallic bonds. With doping Dy into $TbFe_2$, the peak positions show small shift to low *r* (radius distance), which reflects a tiny shortening of the corresponding metallic bonds. The intensities of main peaks rise with increasing Dy content. The results reveal that the structural order of R-Fe and Fe-Fe bonds is improved, that is, the Dy substitution makes the crystal lattice more compact and more ordered than the Tb-rich side. In fact, the $DyFe_2$-type tetragonal structure is the low temperature phase in the MPB compositions in $Tb_{1-x}Dy_xFe_2$ system, while the rhombohedral structure exists at higher temperature. Hence, it's reasonable to assume that the Dy-rich tetragonal phase is energetically more ordered and stable than the rhombohedral one.

To investigate the structural evolutions by temperature, *in-situ* temperature dependent PDF and XRD were performed for $Tb_{0.4}Dy_{0.6}Fe_2$ sample. The PDF patterns displayed in

Figure 2(a) do not show obvious differences on cooling from 300 K to 160 K. This indicates that the $Tb_{0.4}Dy_{0.6}Fe_2$ keeps the rhombohedral local structure within the temperature range, which is consistent with the average structure.[11] The peaks become sharper on cooling due to the weaken of thermal vibration and the increase of structural ordering.

The relation between the rhombohedral cell (pink solid cell) and high temperature cubic cell (teal dashed cell) is shown in Fig. 2(b). In the cell, three Fe_2 atoms configure around one Fe_1 atom forming the Fe_1-Fe_2 bonds, and the same three Fe_2 connect to one R atom via the R-Fe_2 bonds on the opposite direction. The lattice parameters extracted by PDF and XRD analyses are shown in Fig. 2(c) to further investigate the local structure evolutions. The temperature dependent lattice constants (parameter *a* in rhombohedral description) and bond lengths of Fe-Fe, R-Fe_2 and R-R are displayed separately. All parameters decrease with temperature goes down. It's worth noting that the change of *a* gained from PDF is not linear within the temperature range, but shows a slope change at ~220 K, which is marked by two crossed dashed lines in Fig. 2(c). It indicates that the extent of lattice contraction on cooling decreases a little near 220 K. Previous studies[11,14] show that the system would undergo a macroscopic rhombohedral to tetragonal phase transition at much lower temperatures, so the system still own the rhombohedral structure in average when the slope change occurs at ~220 K. More interestingly, we can see the same tendency and slope change in the Fe_1-Fe_2 bond length from Fig. 2(c), while the Fe_2-Fe_2, R-Fe_2 and R-R bond lengths decrease almost linearly from 300 K down to 160 K without any anomalous. It indicates that the Fe_1-Fe_2 bond could be more sensitive to the environment, and it plays an essential role in determining the lattice character of the rhombohedral phase of $Tb_{0.4}Dy_{0.6}Fe_2$. Besides, the lattice constant *a* extracted from XRD shows linear trend which is different from that from PDF, indicating that the slope change of the lattice contraction only occurs at local scale but does not emerge in macroscopic measurements. The lattice constants extracted from PDF and XRD show differences of around 0.02 Å. It is because PDF reflects the structure in local scale where the local undulations in bonds lead to deviations in the lattice parameters from that gained from

average Bragg positions, whose information are reflected by XRD.[28]

The electronic structure and environment around atoms could be affected by substitution and structural change, which could be examined by the x-ray absorption near edge spectra (XANES). Figure 3(a) reports the XANES measured at room temperature at Fe *K*-edge on the Fe foil as reference (dashed line) and on the $Tb_{1-x}Dy_xFe_2$ samples (solid lines). The Fe foil spectrum shows two shoulders near 7114 eV and 7121 eV, and a peak at 7129 eV. The three threshold features can be assigned to the 1*s* to 3*d*, 1*s* to 4*s*, and 1*s* to 4*p* electronic transitions, respectively.[29] Compared with Fe foil, the spectra for $Tb_{1-x}Dy_xFe_2$ samples all show a well-defined pre-edge low-energy peak at ~7112 eV, a shoulderlike main peak at ~7123 eV.

The Fe *K*-edge reflects the excitation of 1*s* electron to the final 4*p* state, which is highly hybridized with 3*d* orbitals,[30] and the pre-edge spectrum probes the unoccupied *p* density of states (DOS) projected on the absorption atoms.[31] The low-energy peak at ~7112 eV is due to the hybridization between the empty Fe 4*p* and 3*d* states at the Fermi level, where the peak intensity reflects the unoccupied 3*d*(4*p*) DOS above the Fermi energy as reported by calculations[32-34] and experiments[35-37]. With increasing the Dy content, the Fe *K*-edge threshold shifts to a little higher energy, and the intensity of the low-energy peak decreases while the main peak show inapparent increase within the experimental resolution. The results indicate the existence of strong electronic perturbation on the DOS driven by Dy substitution. The shift of the edge is due to the shift of Fermi level and the decrease of the peak intensity indicates that the local DOS of 3*d*(4*p*) projected on the Fe sites is reduced.[31,35] The variation in the peak intensities can be interpreted as the gradual filling of the hybridized band among the Fe 3*d* and the R 4*f* and 5*d* states as Dy carries more 4*f* electron than Tb, leading to an increased density of delocalized states above the Fermi level and enhanced 3*d*-4*f*-5*d* hybridization.[38,39] The enhanced hybridization, even to a small extent, could lead to a shortening in the related metallic bonds,[40] which makes the Dy-rich structure more compact.

The extended x-ray absorption fine structure (EXAFS) were performed to examine the

effect of electronic transitions on the bonds and the Fourier transform analysis of Fe *K*-edge EXAFS is shown in Fig. 3(b). Four peaks can be seen from the figure corresponding to different metallic bonds: peaks at ~2.16Å, 4.18 Å and 5.1 Å are due to the first, second and third nearest neighbor Fe-Fe shells including both Fe_1-Fe_2 and Fe_2-Fe_2 with close bond lengths, and the peak at ~2.78 Å represents the R-Fe_2 bonds. Since the phase shift and correction were not included in the analysis, the displayed peaks are at shorter distances than those in real structures and in PDF results. Comparing the spectra of three samples, one can observe that with increasing Dy content in $TbFe_2$, the R-Fe_2 peak intensity raises a lot while the Fe-Fe peaks don't change much. The increase of R-Fe_2 peak reflects the decrease of Debye-Waller factor, which describes the structural and vibrational disorder in the system.[41] It turns out that the crystal lattice becomes more ordered from Tb-rich rhombohedral phase to Dy-rich tetragonal phase with increasing Dy, which is consistent with PDF and XANES results above.

The XAS results show that the Dy substitution leads to stronger 3*d*-4*f*-5*d* hybridization between R and Fe atoms and higher structural order of system. Previous work[40] suggests that stronger hybridization is contributed to the shortening of metallic bonds. Hence, the tetragonal structure induced by Dy substitution should be more ordered and compact than the Tb-rich rhombohedral structure. In the tetragonal case, the bond lengths between the nearest neighbor Fe atoms are almost the same, just like the similar system $Tb_{1-x}Dy_xCo_2$.[42] However, in the rhombohedral phase the Fe_1-Fe_2 bond is longer than Fe_2-Fe_2 bond (2.614 Å to 2.601 Å at 300 K). The interaction between Fe_1-Fe_2 atoms is consequently weaker than that between Fe_2-Fe_2 atoms, which makes it easier to be affected by local environments. Ma *et al*.[14] reported the existing of tetragonal nanodomains in rhombohedral matrix in $Tb_{1-x}Dy_xFe_2$ system at temperatures higher than the MPB temperatures. The existence of domains with different crystal structure from the matrix brings in defects and disorders, which produce local stress and rest the system in a metastable state. The rhombohedral lattice, especially the weak Fe_1-Fe_2 bonds, could be strongly affected by the tetragonal domains and local stress on cooling, and finally lead to the anomalous behavior in the

lattice constant together with Fe_1-Fe_2 bond length in $Tb_{0.4}Dy_{0.6}Fe_2$ case. The effect occurs only at local area where local stress exists; hence it could be the reason why the anomalous behavior is detected only by PDF which focuses on local range, but not observed in XRD which reveals the average crystal information.

IV. CONCLUSIONS

In summary, we studied the local structure in the $Tb_{1-x}Dy_xFe_2$ system by using PDF and XAS techniques. Our results indicate that the system shows the same local structure symmetry with the average structure, and the $Tb_{0.4}Dy_{0.6}Fe_2$ sample keeps rhombohedral on cooling until ~160 K. However, the change of lattice constant is not linear and the distortion is obstructed at ~220 K, which could be related to the effects on weak Fe_1-Fe_2 bond from the local stress induced by local tetragonal domains. The tetragonal structure in Dy-rich side is more ordered than Tb-rich rhombohedral structure based on the XAS results. Our study provides structural information for $Tb_{1-x}Dy_xFe_2$ system in local scale and shows factors influencing the magnetostrictive effect from the local structural view.

SUPPLEMENTARY MATERIAL

The additional data that supports the findings of this study are available within the supplementary material.

ACKNOWLEDGEMENTS

We thank Ronghui Kou for data acquirement and analysis at beamline 20-BM. This research was funded by the National Natural Science Foundation of China (91963111, 51601140, 51701149), the Fundamental Research Funds for the Central Universities (China), the World-Class Universities (Disciplines), the National Science Basic Research Plan in Shaanxi Province of China (2018JM5168). Use of the Advanced Photon Source, an Office of Science User Facility operated for the U.S. Department of Energy (DOE) Office of Science by Argonne National Laboratory, is supported by the U.S. DOE under Contract

No. DE-AC02-06CH11357. Sector 20 is also partially supported by the Canadian Light Source. NSF's ChemMatCARS Sector 15 is supported by the Divisions of Chemistry (CHE) and Materials Research (DMR), National Science Foundation, under grant No. NSF/CHE-1834750.

REFERENCES

1 A. E. Clark and H. S. Belson, Phys. Rev. B **5**, 3642 (1972).

2 H. D. Chopra and M. Wuttig, Nature **521**, 340 (2015).

3 B. Nafradi, T. Keller, F. Hardy, C. Meingast, A. Erb, and B. Keimer, Phys. Rev. Lett. **116**, 047001 (2016).

4 B. Barbara, J. P. Giraud, J. Laforest, R. Lemaire, E. Siaud, and J. Schweizer, Physica B+C **86-88**, 155 (1977).

5 E. Gratz, A. Lindbaum, A. Markosyan, H. Mueller, and A. Y. Sokolov, J. Phys. Condens. Matter **6**, 6699 (1994).

6 S. B. Roy, G. K. Perkins, M. K. Chattopadhyay, A. K. Nigam, K. J. Sokhey, P. Chaddah, A. D. Caplin, and L. F. Cohen, Phys. Rev. Lett. **92**, 147203 (2004).

7 S. Yang and X. Ren, Phys. Rev. B **77**, 014407 (2008).

8 Z. Nie, S. Yang, Y. Wang, Z. Wang, D. Liu, Y. Ren, T. Chang, and R. Zhang, J. Alloys Compd. **658**, 372 (2016).

9 Z. Nie, S. Yang, Y. Wang, Z. Wang, D. Liu, and Y. Ren, Appl. Phys. Letts. **103**, 111903 (2013).

10 S. Yang, H. Bao, C. Zhou, Y. Wang, X. Ren, Y. Matsushita, Y. Katsuya, M. Tanaka, K. Kobayashi, X. Song, and J. Gao, Phys. Rev. Lett. **104**, 197201 (2010).

11 R. Bergstrom, Jr., M. Wuttig, J. Cullen, P. Zavalij, R. Briber, C. Dennis, V. O. Garlea, and M. Laver, Phys. Rev. Lett. **111**, 017203 (2013).

12 C. Zhou, S. Ren, H. Bao, S. Yang, Y. Yao, Y. Ji, X. Ren, Y. Matsushita, Y. Katsuya, M. Tanaka, and K. Kobayashi, Phys. Rev. B **89**, 100101(R) (2014).

13 M. Adil, S. Yang, M. Mi, C. Zhou, J. Wang, R. Zhang, X. Liao, Y. Wang, X. Ren, X. Song, and Y. Ren, Appl. Phys. Letts. **106**, 132403 (2015).

14 T. Ma, X. Liu, X. Pan, X. Li, Y. Jiang, M. Yan, H. Li, M. Fang, and X. Ren, Appl. Phys. Letts. **105**, 192407 (2014).

15 T. Ma, S. Hu, G. Bai, M. Yan, Y. Lu, H. Li, X. Peng, and X. Ren, Appl. Phys. Letts. **106**, 112401 (2015).

16 H. Wang, Y. N. Zhang, T. Yang, Z. D. Zhang, L. Z. Sun, and R. Q. Wu, Appl. Phys. Letts. **97**, 262505 (2010).

17 J. Boisse, H. Zapolsky, and A. G. Khachaturyan, Acta Mater. **59**, 2656 (2011).

18 P. J. Chupas, S. Chaudhuri, J. C. Hanson, X. Qiu, P. L. Lee, S. D. Shastri, S. J. L. Billinge, and C. P. Grey, J. Am. Chem. Soc. **126**, 4756 (2004).

19 F. Bridges, T. Keiber, P. Juhas, S. J. Billinge, L. Sutton, J. Wilde, and G. R. Kowach, Phys. Rev. Lett. **112**, 045505 (2014).

20 D. Xu, C. J. Sun, J. Chen, T. Zhou, S. M. Heald, A. Bergman, B. Sanyal, and G. M. Chow, J. Appl. Phys. **116**, 143902 (2014).

21 M. P. Ruffoni, S. Pascarelli, R. Grossinger, R. S. Turtelli, C. Bormio-Nunes, and R. F. Pettifer, Phys. Rev. Lett. **101**, 147202 (2008).

22 S. Pascarelli, M. P. Ruffoni, R. Sato Turtelli, F. Kubel, and R. Grössinger, Phys. Rev. B **77**, 184406 (2008).

23 B. H. Toby, J. Appl. Crystallogr. **34**, 210 (2001).

24 A. C. Larson and R. B. Von Dreele, Los Alamos National Laboratory Report LAUR **86**, 748 (2004).

25 C. Farrow, P. Juhas, J. Liu, D. Bryndin, E. Božin, J. Bloch, T. Proffen, and S. Billinge, J. Phys. Condens. Matter **19**, 335219 (2007).

26 B. Ravel and M. Newville, J. Synchrotron Radiat. **12**, 537 (2005).

27 U. Atzmony, M. P. Dariel, and G. Dublon, Phys. Rev. B **15**, 3565 (1977).

28 R. Saravanan and M. C. Robert, J. Alloys Compd. **479**, 26 (2009).

29 H. Purdum, P. A. Montano, G. K. Shenoy, and T. Morrison, Phys. Rev. B **25**, 4412 (1982).

30 C.-J. Sun, D. Xu, S. M. Heald, J. Chen, and G.-M. Chow, Phys. Rev. B **84**, 140408(R) (2011).

31 J. Chaboy, C. Piquer, L. M. García, F. Bartolomé, H. Wada, H. Maruyama, and N. Kawamura, Phys. Rev. B **62,** 468 (2000).

32 J. Igarashi and K. Hirai, Phys. Rev. B **50,** 17820 (1994).

33 J. Igarashi and K. Hirai, Phys. Rev. B **53,** 6442 (1996).

34 A. Yanase, J. Phys. F: Met. Phys. **16**, 1501 (1986).

35 J. Chaboy, J. García, and A. Marcelli, J. Magn. Magn. Mater. **166,** 149 (1997).

36 J. Chaboy, A. Marcelli, L. Bozukov, F. Baudelet, E. Dartyge, A. Fontaine, and S. J. P. R. B. Pizzini, Phys. Rev. B **51,** 9005 (1995).

37 N. Ishimatsu, S. Miyamoto, H. Maruyama, J. Chaboy, M. A. Laguna-Marco, and N. Kawamura, Phys. Rev. B **75,** 180402 (2007).

38 G. Fernández, M. G. Berisso, O. Trovarelli, and J. Sereni, J. Alloys Compd. **261,** 26 (1997).

39 M. A. Laguna-Marco, J. Chaboy, and C. Piquer, Phys. Rev. B **77** (2008).

40 R. H. Kou, J. Gao, Y. Ren, S. M. Heald, B. L. Fisher, and C. J. Sun, IEEE Trans. Magn. **54,** 1 (2018).

41 G. Dalba and P. Fornasini, J. Synchrotron Radiat. **4,** 243 (1997).

42 T. Chang, C. Zhou, J. Mi, K. Chen, F. Tian, Y. S. Chen, S. G. Wang, Y. Ren, D. E. Brown, X. Song, and S. Yang, J. Phys. Condens. Matter **32,** 135802 (2019).

FIGURE CAPTIONS

FIG. 1 (a) Refined room temperature XRD results for $Tb_{0.4}Dy_{0.6}Fe_2$; (b) Room temperature PDF results for $Tb_{1-x}Dy_xFe_2$ samples.

FIG. 2 (a) Temperature dependent PDF for $Tb_{0.4}Dy_{0.6}Fe_2$; (b) The rhombohedral cell (pink solid) and cubic cell (teal dashed) for $Tb_{1-x}Dy_xFe_2$; (c) Temperature dependent lattice constants and bond lengths for $Tb_{0.4}Dy_{0.6}Fe_2$.

FIG. 3 (a) Room temperature Fe *K*-edge XANES spectra for Fe foil and $Tb_{1-x}Dy_xFe_2$ samples. (b) Room temperature Fe *K*-edge EXAFS spectra for $Tb_{1-x}Dy_xFe_2$.

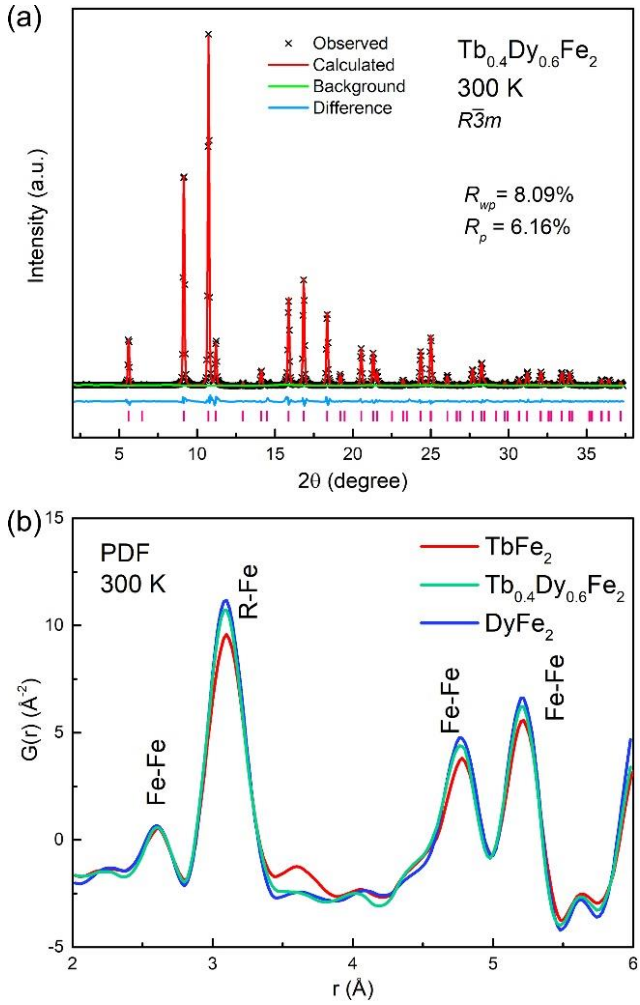
(a)
Observed
Calculated
Background
Difference
Tb0.4Dy0.6Fe2
300 K
R3̄m
Rwp = 8.09%
Rp = 6.16%
Intensity (a.u.)
2θ (degree)
(b)
PDF
300 K
TbFe2
Tb0.4Dy0.6Fe2
DyFe2
R-Fe
Fe-Fe
Fe-Fe
Fe-Fe
G(r) (Å-2)
r (Å)

FIG. 1

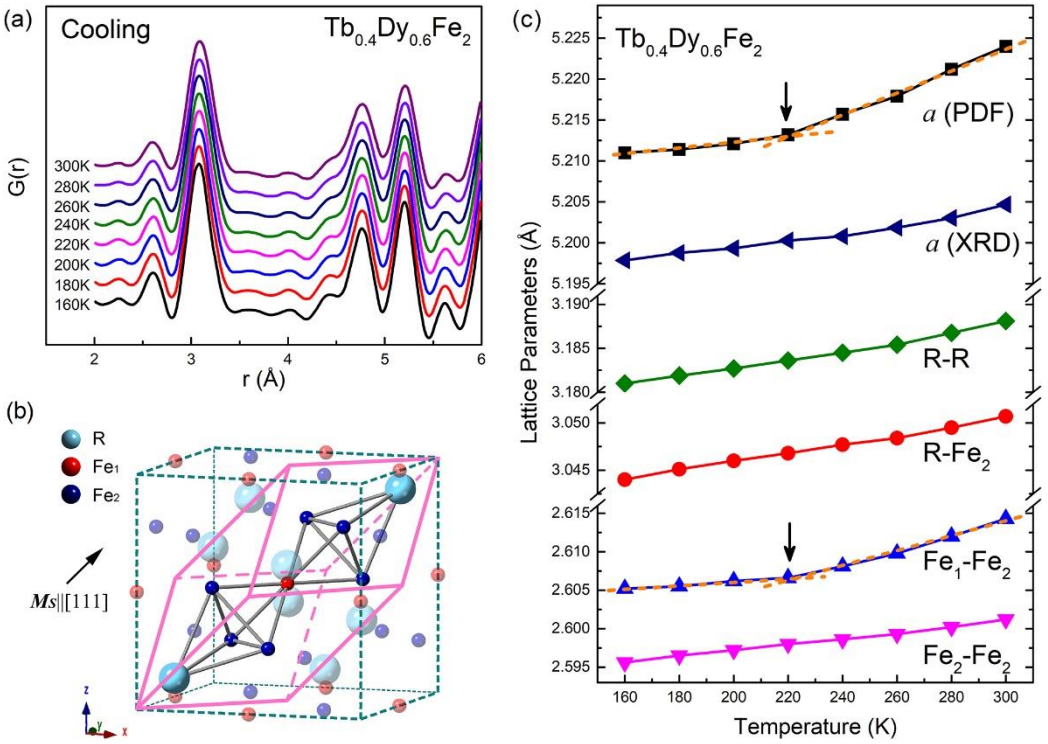
(a)
Cooling
$Tb_{0.4}Dy_{0.6}Fe_2$
G(r)
300K
280K
260K
240K
220K
200K
180K
160K
2
3
4
5
6
r (Å)
(b)
R
Fe1
Fe2
Ms||[111]
z
y
x
(c)
$Tb_{0.4}Dy_{0.6}Fe_2$
Lattice Parameters (Å)
5.225
5.220
5.215
5.210
5.205
5.200
5.195
3.190
3.185
3.180
3.050
3.045
2.615
2.610
2.605
2.600
2.595
a (PDF)
a (XRD)
R-R
R-Fe2
Fe1-Fe2
Fe2-Fe2
160
180
200
220
240
260
280
300
Temperature (K)

FIG. 2

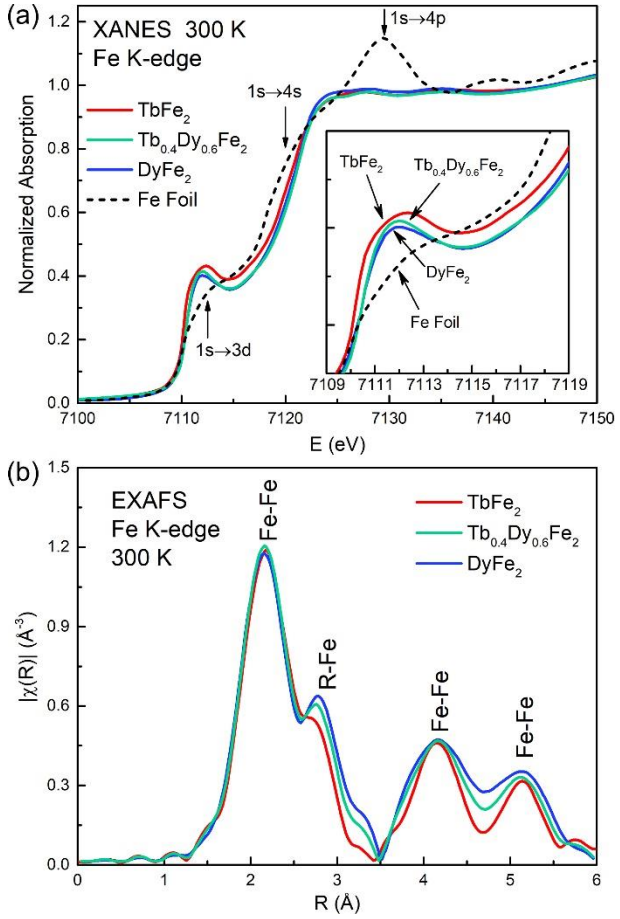
(a)
XANES 300 K
Fe K-edge
TbFe2
Tb0.4Dy0.6Fe2
DyFe2
Fe Foil
1s→4p
1s→4s
1s→3d
Normalized Absorption
E (eV)
(b)
EXAFS
Fe K-edge
300 K
Fe-Fe
R-Fe
Fe-Fe
Fe-Fe
|χ(R)| (Å-3)
R (Å)

FIG. 3